Letter

From high T_c to low T_c: Multiorbital effects in transition metal oxides

Michael Klett,[1,*] Tilman Schwemmer,[1,*] Sebastian Wolf,[2] Xianxin Wu,[3,4] David Riegler,[1] Andreas Dittmaier,[1] Domenico Di Sante,[5,6] Gang Li,[7,8] Werner Hanke,[1] Stephan Rachel,[2,†] and Ronny Thomale[1,‡]

[1]*Institute for Theoretical Physics, University of Wuerzburg, D-97074 Wuerzburg, Germany*
[2]*School of Physics, University of Melbourne, Parkville, Victoria 3010, Australia*
[3]*Max-Planck-Institut für Festkörperforschung, Heisenbergstrasse 1, D-70569 Stuttgart, Germany*
[4]*CAS Key Laboratory of Theoretical Physics, Institute of Theoretical Physics, Chinese Academy of Sciences, Beijing 100190, China*
[5]*Department of Physics and Astronomy, University of Bologna, Bologna, Italy*
[6]*Center for Computational Quantum Physics, Flatiron Institute, New York, NY 10010, USA*
[7]*School of Physical Science and Technology, ShanghaiTech University, Shanghai 201210, China*
[8]*ShanghaiTech Laboratory for Topological Physics, ShanghaiTech University, Shanghai 201210, China*

(Received 12 January 2021; accepted 18 August 2021; published 14 September 2021)

Despite the structural resemblance of certain cuprate and nickelate parent compounds there is a striking spread of T_c among such transition metal oxide superconductors. We adopt a minimal two-orbital e_g model which covers cuprates and nickelate heterostructures in different parametric limits, and analyze its superconducting instabilities. The joint consideration of interactions, doping, fermiology, and in particular the e_g orbital splitting allows us to explain the strongly differing pairing propensities in cuprate and nickelate superconductors.

DOI: 10.1103/PhysRevB.104.L100502

Introduction. High-temperature unconventional superconductivity, as discovered in copper oxides in 1986 [1], has ever since decisively framed the landscape of research in condensed matter physics. In particular, many trends of T_c as a function of tunable system parameters have been investigated. The hope is to identify a way to tune the cuprates just enough to approach room temperature, and hence render them, or another class of unconventional superconductors, technologically viable [2,3]. Initially, the rather accurate single-orbital one-band Hubbard model description was assumed to be an advantageous, and hence already T_c optimized, feature of the copper oxide superconductors. Due to the Jahn-Teller effect, the apical oxygen distance to the CuO_2 planes is elongated, and thus ensures a splitting of the e_g orbitals such that the $3d^9$ configuration of Cu yields a nearly exclusive hole population of the $3d_{x^2-y^2}$ orbital [4].

Research on unconventional superconductivity over the past two decades indicates that this picture, in its generality, needs revision [5]. While orbital fluctuations may be detrimental to high T_c, multiorbital systems can also yield beneficial effects for unconventional superconductivity, such as the multipocket fermiology of iron-based superconductors [6,7]. Interpreting the single-band cuprates as the nucleus for high-T_c superconductivity, the addition of multiorbital character can thus take different turns. Nickelate thin-film heterostructures such as $LaNiO_3/LaAlO_3$, whose electronic structure is suggested to be analogous to the high-T_c cuprate compounds [8,9], only show a T_c as low as 3 K [10]. This might hint at the detrimental effect of orbital fluctuations, which would be in line with a precise analysis of the impact of interactions on the orbital polarization [11]. We call this a low-T_c instance of multiorbital effects. To the contrary, $Ba_2CuO_{3+\delta}$, where e_g orbital fluctuations are likewise expected to be as prominently present as in $LaNiO_3$ heterostructures, reaches a T_c as high as 70 K [12], which we highlight as a high-T_c instance. Note that all aforementioned material examples of transition metal oxide superconductors are characterized by the e_g orbitals of the transition metal atom at low energies, albeit for different orbital fillings (Ni $3d^7$ versus Cu $3d^9$), doping levels, and Fermi surface topologies (fermiologies). Adopting the view from a generalized e_g two-orbital octahedral oxide setting, $Ba_2CuO_{3+\delta}$ has recently been speculated [12] to drastically modify the e_g splitting due to a strong reduction of the apical oxygen distance, bringing into play both the $3d_{x^2-y^2}$ and $3d_{3z^2-r^2}$ orbital.

In this Letter, we particularize on the analysis of an effective two-band model spanned by the e_g orbital space of transition metal oxides, and investigate the onset of superconducting order. While variants of this model have already been studied in the context of overdoped cuprate superconductors in general [13] and $Ba_2CuO_{3+\delta}$ in particular [14], we create a synoptic perspective on multiorbital effects by comparing the high-T_c material $Ba_2CuO_{3+\delta}$ (BCO) to the low-T_c regime of $LaNiO_3/LaAlO_3$ (LNO/LAO) heterostructures. The rare-earth nickelates, with a close similarity between the NiO_2 and CuO_2 planes, have recently surfaced as potentially cuprate-related unconventional superconductors [15] and, since the finding of T_c up to 15 K in $NdNiO_2$, have established an exciting domain, in which even higher T_c's may be realized [16]. An earlier idea in this direction [8], followed up by local density approximation (LDA)+ dynamical mean-field theory (DMFT) electronic structure calculations [9], suggested turning a nickelate Fermi surface (FS) into a cupratelike one

*These authors contributed equally to this work.
†stephan.rachel@unimelb.edu.au
‡rthomale@physik.uni-wuerzburg.de

by orbital engineering via heterostructuring: sandwiching a $LaNiO_3$ layer between layers of an insulating oxide, such as $LaAlO_3$, will confine the $3d_{3z^2-r^2}$ orbital in the z direction, removing this band from the FS. This way, one restricts the electron to the $3d_{x^2-y^2}$ orbital, similar to the conventional cuprate case. The DMFT calculation of Ref. [9] yields a single-sheet FS with a small (30%) $3d_{3z^2-r^2}$ component. The more recent experimental finding of a T_c of only 3K in related heterostructures, however, challenges the hitherto belief that T_c is optimized when the $3d_{x^2-y^2}$ orbital weight is concentrated in a single band.

Following up on previous work, we compare the high-T_c to the low-T_c regime of the e_g two-orbital Hubbard model by employing a toolkit composed of a variety of numerical methods. Our analysis is performed through Kohn-Luttinger (KL)-type calculations [17–19] in the weak-coupling regime and through functional renormalization group (FRG) [7,20] as well as random phase approximation (RPA) [21–23] studies in the intermediate-coupling regime. We find that, most importantly, the e_g energy splitting and the orbital filling turn out to be crucial parameters to unravel different superconducting orders, and drastically varying pairing strengths. All methods yield d-wave and extended s-wave pairing as the leading and subleading superconducting orders in the high-T_c regime. The ordering hierarchy in the low-T_c regime becomes significantly more susceptible to even a small change of parameters, and hence less universal.

e_g minimal model. The shared geometry of the TO_2 (T = Ni, Cu) planes leads to similarities of the ratios of different transition matrix elements $t_{o'o,\alpha}$ between neighboring sites, as established by *ab initio* density functional theory (DFT) calculations [24] yielding band structures such as Fig. 1. This allows us to identify two critical parameters that distinguish the high-T_c material BCO from the low-T_c nickelate heterostructure. The first is the e_g manifold splitting ϵ caused by Jahn-Teller distortions of the oxygen octahedra, which is significantly enhanced in the cuprate system (0.87 eV) compared to the nickelate system (0.11 eV). The second crucial distinction, which is particularly visible through the paradigmatic material limits of cuprates and nickelates, is given by the doping level δ. While the transition metal ion in both cases is nominally given by $3d^7$ for LNO/LAO and Ba_2CuO_4, reducing the oxygen doping in BCO δ will increase the filling of the d shell up to a $3d^9$ configuration for Ba_2CuO_3. In our model, this is taken into account by increasing the filling of the e_g subspace for BCO to $n = 2$ electrons. The Hamiltonian we adopt for both materials (albeit with different parameters) is given by

$$H_0 = \sum_{i,\sigma}\sum_{o=1,2}\left((-1)^o\frac{\epsilon}{2} - \mu\right)c^\dagger_{o,i,\sigma}c_{o,i,\sigma} + \sum_{i,\sigma}\sum_{j\neq i}\sum_{o',o=1,2} t_{o'o,\alpha(i,j)}c^\dagger_{o',i,\sigma}c_{o,j,\sigma}, \quad (1)$$

where $c^\dagger_{o,i}$ creates an electron in the orbital $o = 1, 2$ ($d_{x^2-y^2}$, $d_{3z^2-r^2}$) on site $\vec{r}_i$. The index $\alpha(i, j)$ counts the proximity of different sites i and j and is used to label the corresponding orbital hybridizations $t_{o'o,\alpha}$; ϵ indicates the size of the on-site energy difference for the relevant orbitals and the chemical potential μ controls the filling of the system.

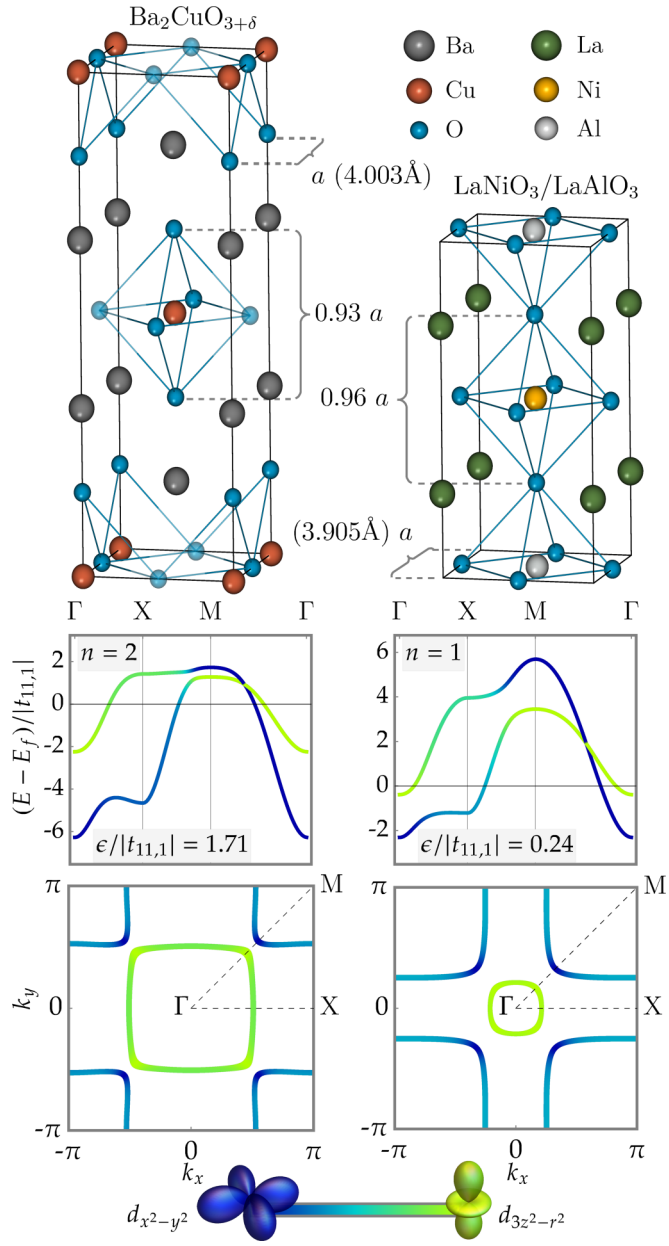

FIG. 1. Sketch of unit cell, band structure, and Fermi surface for BCO (unit cell for $\delta = 1$, left) and LNO/LAO (right). The orbital weight of a state is given by the respective color blend of blue ($d_{x^2-y^2}$) and green ($d_{3z^2-r^2}$); we indicate the density of states on the Fermi surface by the thickness of the line.

Starting from DFT calculations [25,26] for our prototypical material instances LNO/LAO and BCO, the tight-binding parameters for this low-energy model were obtained by projecting the DFT result onto a pair of maximally localized Wannier orbitals on the transition metal ions [27]. The resulting model parameters for both LNO heterostructures and BCO are given in the Supplemental Material (SM) [24].

Despite the different material chemistry, the similarity of the obtained parameter sets after normalizing to the bandwidth is remarkable, given the strongly differing T_c. We are able to identify two significant differences: (i) the orbital splitting and (ii) the filling fraction of the e_g doublet. While the orbital splitting mainly controls the energy splitting of the bands at

the Γ point as well as the orbital hybridization, the resulting differences in the fermiology, seen in Fig. 1, result primarily from the difference in the chemical potential.

We model the interaction by adopting a Kanamori-type Hamiltonian, comprising the four on-site interaction terms in the considered multiorbital model:

$$\begin{aligned} H_I = & U \sum_{i,o} c^\dagger_{o,i,\uparrow} c_{o,i,\uparrow} c^\dagger_{o,i,\downarrow} c_{o,i,\downarrow} \\ & + V \sum_{i,\sigma,\sigma'} c^\dagger_{1,i,\sigma} c_{1,i,\sigma} c^\dagger_{2,i,\sigma'} c_{2,i,\sigma'} \\ & + J \sum_{i,\sigma,\sigma'} c^\dagger_{1,i,\sigma} c^\dagger_{2,i,\sigma'} c_{1,i,\sigma'} c_{2,i,\sigma} \\ & + J' \sum_{i,o\neq o'} c^\dagger_{o,i,\uparrow} c^\dagger_{o,i,\downarrow} c_{o',i,\downarrow} c_{o',i,\uparrow}, \end{aligned} \tag{2}$$

with intraorbital (U) and interorbital (V) repulsive interactions as well as Hund's coupling (J) and pair hopping terms (J'). The orbital makeup of the BCO bands at the Fermi level are cleaner than the ones of LNO/LAO due to the larger orbital splitting ϵ. As a consequence, interorbital (intraorbital) interactions and interpocket (intrapocket)/band interactions correlate more strongly in the case of BCO compared to LNO/LAO.

Assuming rotational symmetry for the interaction, as well as a perfectly degenerate e_g orbital manifold, these parameters are restricted by $V = U - 2J$ and $J' = J$ [28–31]. We further fix $J = 0.25\,U$ (resulting in $V = U/2$) and are subsequently left with the overall interaction scale U as the only free parameter.

Since the cubic symmetry of the e_g complex is broken by the Jahn-Teller splitting ϵ and the anisotropy in the screened Coulomb interaction, it is interesting to compare interaction schemes beyond this simple modeling [30]. The ratio of inter- versus intraorbital interaction strength hence is a reasonable parameter to explore, and we further use it to gain additional insight into multiorbital interaction effects in our effective model. While actual materials will be limited to the vicinity of $V/U \approx 1/2$, it is revealing to fully probe the available parameter space, as implemented in the SM [24]. For the remainder of the main text, we fix $V = U/2$ and choose a bare value of $U = 3.5$ eV for the functional renormalization group calculations in both models [32], resulting in a value of $U/W = 0.86$ (0.98) for BCO (LNO/LAO) (for further details regarding all methods see also the SM [24]).

Results. In order to get a first impression of the primary spin fluctuation channels, we analyze the bare particle-hole susceptibility,

$$\begin{aligned} \chi_0(\boldsymbol{q}, \omega) &= \sum_{oo'} \sum_{\boldsymbol{k}, i\tilde{\omega}_n} \left(G^{oo'}_{\boldsymbol{k}+\boldsymbol{q}, \omega+i\tilde{\omega}_n} G^{o'o}_{\boldsymbol{k}, i\tilde{\omega}_n} \right) \\ &= \sum_{oo'} \chi^{oo'}(\boldsymbol{q}, \omega). \end{aligned} \tag{3}$$

It is determined by the single-particle Green's functions $G^{oo'}_{\boldsymbol{k}, i\omega_n}$ and hence independent of the employed approximations for the treatment of interactions beyond DFT. We show its zero frequency limit in Fig. 2 and highlight corresponding nesting features of the Fermi surface. In contrast to LNO/LAO, which shows an overall uniform bare susceptibility, the nesting in BCO is strongly enhanced for the transfer momenta $\boldsymbol{Q}_1 = (\pi, 0), (0, \pi)$ and $\boldsymbol{Q}_2 = (\pi, \pi)$. These commensurate nesting vectors induce pronounced spin fluctuations in the system which will finally result in attractive interaction channels for the pair-scattering vertex (see, e.g., Ref. [3]).

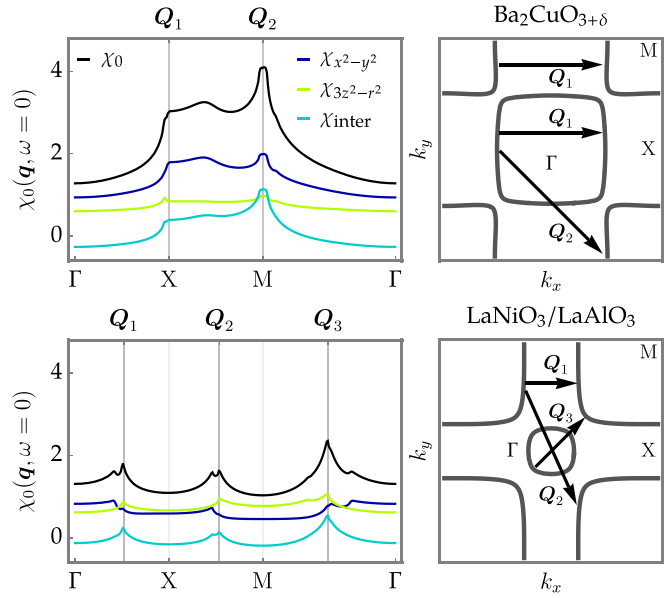

FIG. 2. Bare susceptibility in arbitrary units for BCO (top) and LNO/LAO (bottom) with $\chi^{11} = \chi_{x^2-y^2}$, $\chi^{22} = \chi_{3z^2-r^2}$, and $\chi^{12} + \chi^{21} = \chi_{\text{inter}}$ and leading nesting vectors shown in the corresponding Brillouin zone (right-hand side).

While analyzing the onset of superconductivity for LNO/LAO and BCO one has to be particularly careful due to strong correlation effects in the transition metal oxides [33]. Accordingly we triangulate the problem through different methods: (i) a Kohn-Luttinger-type analysis [17,18], which is asymptotically exact at infinitesimal coupling, (ii) complemented by a standard random phase approximation [21–23], as well as (iii) functional renormalization group [7,20] calculations.

In the main text, we constrain ourselves mainly to the presentation of the FRG results, and refer the reader to the detailed SM for additional information [24]. Since the material instances are most likely located in the intermediate-coupling regime, the FRG provides the most systematic treatment of superconductivity, as it treats all particle-hole and particle-particle channels on equal footing.

It thus allows to most directly resolve the connection between spin fluctuations and superconductivity, as has been shown in numerous studies (e.g., Refs. [7,20]). Still, one needs to stay aware of the fact that all numerical methods at intermediate coupling are just approximations. Due to this, we also added the Kohn-Luttinger analysis, in order to have a rigorous reference point at infinitesimal coupling [34].

Within FRG, we determine the critical cutoff energy Λ_c and effective two-particle irreducible vertex $\Gamma^{\Lambda_c}(\boldsymbol{k}_1, \boldsymbol{k}_2, \boldsymbol{k}_3, \boldsymbol{k}_4)$ for our effective model. As with all other methods used, a short review of the FRG methodology is delegated to the SM [24]. The renormalization flow breaks

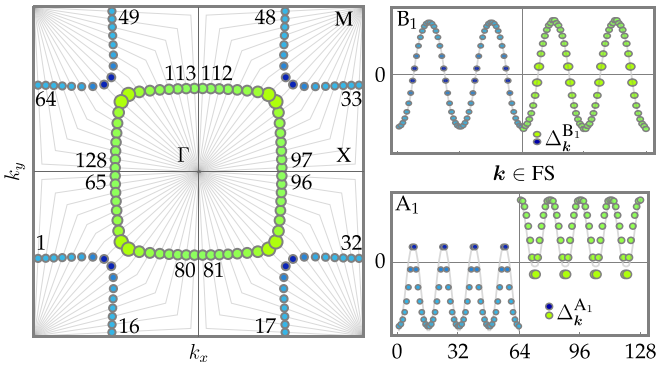

FIG. 3. Fermi surface (left) of BCO discretized in patches (1–128) for the numerical FRG study. The color scheme, representing the orbital weights, is in accordance with Fig. 1 and the thickness of the plot marker indicates the density of states. On the right-hand side we plotted the form factor of the leading (upper panel) and subleading (lower panel) eigenvalue λ for the superconducting channel on the discretized Fermi surface at the breakdown of the FRG flow. They transform according to the B_1 and A_1 irreducible representations of the lattices' C_{4v} point-group symmetry, respectively. The fitted harmonic fingerprint of these form factors is indicated by the grey lines in the panels on the right.

down at Λ_c; i.e., the entries of Γ^{Λ_c} diverge so that we can classify the leading instability by decomposing the full effective vertex Γ^{Λ_c} into mean-field channels. For superconductivity, we obtain the effective Cooper pair interaction $\Gamma^{\mathrm{SC},\Lambda_c}(\boldsymbol{k},\boldsymbol{k}') = \Gamma^{\Lambda_c}(\boldsymbol{k},-\boldsymbol{k},\boldsymbol{k}',-\boldsymbol{k}')$. By solving the linearized gap equation

$$\lambda\Delta_{\boldsymbol{k}} = \sum_{\boldsymbol{k}'} \Gamma^{\mathrm{SC},\Lambda_c}(\boldsymbol{k},\boldsymbol{k}')\Delta_{\boldsymbol{k}'} \tag{4}$$

with $\Lambda_c \propto T_c$, we identify the symmetry class of the superconducting gap function $\Delta_{\boldsymbol{k}}$ for the smallest eigenvalue λ at Λ_c.

Figure 3 displays the gap functions for the leading and subleading eigenvalues λ for BCO. We find a cuprate-like $d_{x^2-y^2}$-wave form factor for the leading eigenvalue of $\Gamma^{\mathrm{SC},\Lambda_c}(\boldsymbol{k},\boldsymbol{k}')$ and extended s-wave order for the subleading eigenvalue. Assigning the associated irreducible lattice representation (irrep), the leading eigenvalue possesses the symmetry character B_1 with $\Delta_{\boldsymbol{k}}^{B_1} \propto (\cos k_x - \cos k_y) + 0.001\,(\cos 2k_x - \cos 2k_y)$ and the subleading one A_1 with $\Delta_{\boldsymbol{k}}^{A_1} \propto (\cos k_x + \cos k_y) + 0.45\,(\cos 3k_x + \cos 3k_y)$. The harmonic decomposition of these form factors is obtained by fitting to the FRG eigenvectors. For BCO, these results agree with the RPA results presented in the SM [24], which in turn reproduce previous RPA results by Maier *et al.* [14].

It is quite transparent in FRG how these superconducting orders relate to the pronounced spin fluctuation channels: the B_1 and A_1 form factors are enhanced by the dominant pair scattering process with momentum transfer $\boldsymbol{Q}_2$, and partially by $\boldsymbol{Q}_1$. The corners of the Fermi surface are favorably nested to a majority of the momenta on the same Fermi pocket via $\boldsymbol{Q}_1$ and the corners of the other Fermi pocket via $\boldsymbol{Q}_2$, yielding additional nodes and a particularly anisotropic A_1 form factor.

TABLE I. Ratio of the critical temperature for LNO/LAO and BCO calculated by FRG, RPA, and KL analysis and the corresponding classification of the gap function in irreducible lattice representations (irreps). The irreps are often named according to their nodal structure: A_1 is referred to as an (extended) s wave, E as a p wave, and B_1 (B_2) as $d_{x^2-y^2}$ (d_{xy}).

Method	$T_c^{LNO/LAO}/T_c^{BCO}$	(sub)leading irrep	
		BCO	LNO/LAO
fRG	10^{-2}	B_1 (A_1)	E (B_2)
RPA	10^{-10}	B_1 (A_1)	B_2 (B_1)
KL	10^{-11700}	A_1 (B_1)	B_2 (B_1)

By contrast, the FRG analysis of LNO/LAO yields an upper bound for T_c which is two orders lower in magnitude, and a form factor transforming under the E irrep of the crystal's point group. The Fermi pockets feature no particularly pronounced nesting which, combined with the unclean orbital makeup, yields a nearly uniform pairwise interaction between different points of the Fermi surface. As a consequence, Λ_c is dramatically decreased compared to the BCO results.

We present the symmetry class of the leading form factor and the ratio of T_c for BCO and LNO/LAO in Table I for the FRG, RPA, and KL calculations. A unanimous finding of all methods is the overall trend of lower T_c for LNO/LAO as well as the leading $d_{x^2-y^2}$- and s-wave instabilities for the high-T_c case in BCO. For LNO/LAO, all methods substantially differ from each other. Given the small instability scale and, from there, the enhanced sensitivity of the result to the specific formulation of the approximative method, this is not surprising. It shows that in the low-T_c, or rather pairing noise, regime, even slight biases of different approximation schemes manage to affect the eventual result, and strongly enhance the volatility of any result for the superconducting instability. Nevertheless, it is still interesting to trace back the biases of the different methods in such a case, which is delegated to the SM [24].

Conclusion. Already in an effective description as simple as the e_g minimal model studied in this work, we can identify the enormous range of multiorbital effects on T_c at the example of a multiorbital high-T_c material $Ba_2CuO_{3+\delta}$ and a multiorbital low-T_c material $LaNiO_3/LaAlO_3$. Certainly, this study is not exhaustive in describing all multiorbital effects in transition metal superconductors. For instance, not only multiple orbitals of the transition metal atom, but also other orbital degrees of freedom may prevail at low energies, such as recently observed for infinite layer nickelates. Still, we expect the minimal modeling of multiorbital effects to constitute a promising future direction to close the gap between experimental evidence and theoretical simulation of unconventional superconductors.

Acknowledgments. This work is funded by the Deutsche Forschungsgemeinschaft (DFG, German Research Foundation) through Project-ID 258499086 - SFB 1170 and through the Würzburg-Dresden Cluster of Excellence on Complexity and Topology in Quantum Matter-ct.qmat Project-ID 390858490 - EXC 2147. S.R. acknowledges support from the Australian Research Council through Gratns No. FT180100211 and No. DP200101118. We further gratefully

acknowledge the Gauss Centre for Supercomputing e.V. [35] for providing computing time on the GCS Supercomputer SuperMUC at Leibniz Supercomputing Centre [36] and the HPC facility Spartan [37] hosted at the University of Melbourne. The research leading to these results has received funding from the European Union's Horizon 2020 research and innovation programme under the Marie Skłodowska-Curie Grant Agreement No. 897276.

[1] J. G. Bednorz and K. A. Müller, Z. Phys. B: Condens. Matter **64**, 189 (1986).
[2] B. Keimer, S. A. Kivelson, M. R. Norman, S. Uchida, and J. Zaanen, Nature (London) **518**, 179 (2015).
[3] D. J. Scalapino, Rev. Mod. Phys. **84**, 1383 (2012).
[4] E. Pavarini, I. Dasgupta, T. Saha-Dasgupta, O. Jepsen, and O. K. Andersen, Phys. Rev. Lett. **87**, 047003 (2001).
[5] H. Sakakibara, H. Usui, K. Kuroki, R. Arita, and H. Aoki, Phys. Rev. Lett. **105**, 057003 (2010).
[6] Q. Si, R. Yu, and E. Abrahams, Nat. Rev. Mater. **1**, 16017 (2016).
[7] C. Platt, W. Hanke, and R. Thomale, Adv. Phys. **62**, 453 (2013).
[8] J. Chaloupka and G. Khaliullin, Phys. Rev. Lett. **100**, 016404 (2008).
[9] P. Hansmann, X. Yang, A. Toschi, G. Khaliullin, O. K. Andersen, and K. Held, Phys. Rev. Lett. **103**, 016401 (2009).
[10] G. Zhou, F. Jiang, J. Zang, Z. Quan, and X. Xu, ACS Appl. Mater. Interfaces **10**, 1463 (2018).
[11] M. J. Han, X. Wang, C. A. Marianetti, and A. J. Millis, Phys. Rev. Lett. **107**, 206804 (2011).
[12] W. M. Li, J. F. Zhao, L. P. Cao, Z. Hu, Q. Z. Huang, X. C. Wang, Y. Liu, G. Q. Zhao, J. Zhang, Q. Q. Liu, R. Z. Yu, Y. W. Long, H. Wu, H. J. Lin, C. T. Chen, Z. Li, Z. Z. Gong, Z. Guguchia, J. S. Kim, G. R. Stewart *et al.*, Proc. Natl. Acad. Sci. USA **116**, 12156 (2019).
[13] K. Jiang, X. Wu, J. Hu, and Z. Wang, Phys. Rev. Lett. **121**, 227002 (2018).
[14] T. Maier, T. Berlijn, and D. J. Scalapino, Phys. Rev. B **99**, 224515 (2019).
[15] X. Wu, D. Di Sante, T. Schwemmer, W. Hanke, H. Y. Hwang, S. Raghu, and R. Thomale, Phys. Rev. B **101**, 060504(R) (2020).
[16] D. Li, K. Lee, B. Wang, M. Osada, S. Crossley, H. Lee, Y. Cui, Y. Hikita, and H. Hwang, Nature (London) **572**, 624 (2019).
[17] W. Kohn and J. M. Luttinger, Phys. Rev. Lett. **15**, 524 (1965).
[18] S. Raghu, S. A. Kivelson, and D. J. Scalapino, Phys. Rev. B **81**, 224505 (2010).
[19] A. V. Chubukov and S. A. Kivelson, Phys. Rev. B **96**, 174514 (2017).
[20] W. Metzner, M. Salmhofer, C. Honerkamp, V. Meden, and K. Schönhammer, Rev. Mod. Phys. **84**, 299 (2012).
[21] N. F. Berk and J. R. Schrieffer, Phys. Rev. Lett. **17**, 433 (1966).
[22] D. J. Scalapino, E. Loh, and J. E. Hirsch, Phys. Rev. B **34**, 8190 (1986).
[23] S. Graser, T. A. Maier, P. J. Hirschfeld, and D. J. Scalapino, New J. Phys. **11**, 025016 (2009).
[24] See Supplemental Material at http://link.aps.org/supplemental/10.1103/PhysRevB.104.L100502 for details on the used minimal e_g model and the utilized methods as well as additional references therein [38–51].
[25] P. Giannozzi, S. Baroni, N. Bonini, M. Calandra, R. Car, C. Cavazzoni, D. Ceresoli, G. L. Chiarotti, M. Cococcioni, I. Dabo, A. D. Corso, S. de Gironcoli, S. Fabris, G. Fratesi, R. Gebauer, U. Gerstmann, C. Gougoussis, A. Kokalj, M. Lazzeri, L. Martin-Samos *et al.*, J. Phys.: Condens. Matter **21**, 395502 (2009).
[26] P. Giannozzi, O. Andreussi, T. Brumme, O. Bunau, M. B. Nardelli, M. Calandra, R. Car, C. Cavazzoni, D. Ceresoli, M. Cococcioni, N. Colonna, I. Carnimeo, A. D. Corso, S. de Gironcoli, P. Delugas, R. A. DiStasio, A. Ferretti, A. Floris, G. Fratesi, G. Fugallo *et al.*, J. Phys.: Condens. Matter **29**, 465901 (2017).
[27] N. Marzari, A. A. Mostofi, J. R. Yates, I. Souza, and D. Vanderbilt, Rev. Mod. Phys. **84**, 1419 (2012).
[28] J. Kanamori, Prog. Theor. Phys. **30**, 275 (1963).
[29] B. Brandow, Adv. Phys. **26**, 651 (1977).
[30] T. Ribic, E. Assmann, A. Tóth, and K. Held, Phys. Rev. B **90**, 165105 (2014).
[31] A. M. Oleś, G. Khaliullin, P. Horsch, and L. F. Feiner, Phys. Rev. B **72**, 214431 (2005).
[32] C. Platt, R. Thomale, and W. Hanke, Phys. Rev. B **84**, 235121 (2011).
[33] S. Lederer, Y. Schattner, E. Berg, and S. A. Kivelson, Phys. Rev. Lett. **114**, 097001 (2015).
[34] R. Shankar, J. Stat. Phys. **103**, 485 (2001).
[35] www.gauss-centre.eu.
[36] www.lrz.de.
[37] L. Lafayette, G. Sauter, L. Vu, and B. Meade, Spartan Performance and Flexibility: An HPC-Cloud Chimera (OpenStack Summit, Barcelona, 2016), doi: 10.4225/49/58ead90dceaaa.
[38] J. P. Perdew, K. Burke, and M. Ernzerhof, Phys. Rev. Lett. **77**, 3865 (1996).
[39] M. Altmeyer, D. Guterding, P. J. Hirschfeld, T. A. Maier, R. Valentí, and D. J. Scalapino, Phys. Rev. B **94**, 214515 (2016).
[40] M. Salmhofer and C. Honerkamp, Prog. Theor. Phys. **105**, 1 (2001).
[41] F. J. Wegner and A. Houghton, Phys. Rev. A **8**, 401 (1973).
[42] J. Polchinski, Nucl. Phys. B **231**, 269 (1984).
[43] C. Wetterich, Phys. Lett. B **301**, 90 (1993).
[44] T. Takimoto, T. Hotta, and K. Ueda, Phys. Rev. B **69**, 104504 (2004).
[45] K. Kubo, Phys. Rev. B **75**, 224509 (2007).
[46] A. F. Kemper, T. A. Maier, S. Graser, H.-P. Cheng, P. J. Hirschfeld, and D. J. Scalapino, New J. Phys. **12**, 073030 (2010).
[47] S. Raghu and S. A. Kivelson, Phys. Rev. B **83**, 094518 (2011).
[48] S. Raghu, E. Berg, A. V. Chubukov, and S. A. Kivelson, Phys. Rev. B **85**, 024516 (2012).
[49] W. Cho, R. Thomale, S. Raghu, and S. A. Kivelson, Phys. Rev. B **88**, 064505 (2013).
[50] S. Wolf, T. L. Schmidt, and S. Rachel, Phys. Rev. B **98**, 174515 (2018).
[51] S. Wolf and S. Rachel, Phys. Rev. B **102**, 174512 (2020).